Fluorescence Up-Conversion Study of Excitation Energy Transport Dynamics in Oligothiophene−Fullerene Linked Dyads

Takumi Nakamura,[†,§] Yasuyuki Araki,[*,†] Osamu Ito,[†] Kazuo Takimiya,[‡] and Tetsuo Otsubo[‡]

Institute of Multidisciplinary Research for Advanced Materials, Tohoku University, Katahira, Sendai, Miyagi 980-8577, Japan, and Department of Applied Chemistry, Graduate School of Engineering, Hiroshima University, Higashi-Hiroshima 739-8527, Japan

Received: October 18, 2007; In Final Form: November 19, 2007

Photoinduced excitation energy transport dynamics in oligothiophene−fullerene linked dyads, *n*T-C_{60} (n = 4, 8, and 12), have been investigated by femtosecond fluorescence up-conversion. In 8T-C_{60} and 12T-C_{60}, each time profile of the fluorescence due to the ^1nT* moiety consists of two components. The sub-picosecond component and a few picosecond components were experimentally evaluated depending on the lengths of oligothiophenes (n =8 and 12) and on the analyzing wavelength of the fluorescence. However, the time trace of the fluorescence due to ^{1}4T*-C_{60} decayed with a single short component in ∼300 fs due to direct excited energy transfer (EET) from the ^{1}4T* moiety to the C_{60} moiety. On the basis of the kinetic models considering the short and long locally π-conjugative thiophene segments in 8T-C_{60} and 12T-C_{60}, the rate parameters of the elemental processes were evaluated. Sub-picosecond time constants of *n*T-C_{60} were found to be EET from the thiophene segment vicinal to the C_{60} moiety and intrachain energy transfer. Slower picosecond dynamics mainly corresponds to EET from the thiophene segments apart from the C_{60} moiety.

1. Introduction

The conjugated nanoscale molecules are useful to design the molecular electronic devices, i.e., electric luminescent devices,[1,2] photovoltaic cells,[3,4] field effect transistors,[5,6] nonlinear optics,[7] and electrical conductors.[8,9] Recently, the photoinduced electron transfer (ET) systems with highly efficient charge-separation and slow charge-recombination processes have been applied to the photovoltaic cells.[10,11] Highly conjugated nanoscale molecular wires are indispensable for single molecular electron devices.[8,9] In π-conjugated polymers, the defects of the π-conjugation generate the structural disorder that leads to the inhomogeneous broadening of the $\pi-\pi^*$ absorption bands. In polythiophene, the π-conjugation is thought to be separated by conformational defects.[12] As many groups already discussed, the excitation-energy transfer (EET) mechanism among the segments is described on the basis of the resonance energy transfer model between the weakly coupled chromophores.[13−16] The initial photoexcitation dynamics of conjugated polymers/oligomers were well-investigated experimentally and theoretically.[13−26] Recently, Sundström and co-workers reported the exciton transfer in a polythiophene in solution revealed by femtosecond transient absorption measurements.[15,16,22] The observed dynamic Stokes shift of the stimulated emission was discussed on the basis of Monte Carlo simulations of resonant energy transfer by line-dipole Förster energy transfer model.[14−16] The vibrational relaxation takes place within ∼100 fs, because the exciton self-trapping strongly couples with the phonon mode of polythiophenes.[14−16] Within 1 ps, the EET occurs from higher-energy oligothiophene segments to lower-energy segments (downhill excitation energy transfer). In addition, the energy migration also occurs between isoenergetic oligothiophene segments in the time range from a few picoseconds to several tens of picoseconds.[14−16] Sundström and co-workers also observed the spectral red-shift due to the torsional relaxation process of polythiophenes.[16] In this process, the conformation changes from the aromatic structure to the quinoid structure, accompanying the changes of the π-conjugation lengths.[16] Photoexcitation dynamics of oligothiophenes (*n*T's) have been investigated by many research groups as components of polythiophene.[27−43] It is well-known that properties of oligothiophenes show a tendency to saturate with an increase in the thiophene units, suggesting the presence of the locally π-conjugative thiophene segments, although the length of the segments slightly increases with the total length of oligothiophenes.[28,29] The highest-occupied molecular orbital−lowest-unoccupied molecular orbital gaps of the oligothiophenes become small with an increase in the thiophene units, which also change oxidation potentials and the energy levels of the excited states.[28−34] Janssen et al. reported that oligothiophenes have considerable rigid planer structures in the lowest excited S_1 state.[35] Lanzani and co-workers investigated initial relaxation dynamics of oligothiophenes with femtosecond time-resolved spectroscopies.[36−39] They observed the dynamical fluorescence band shift toward the red region with relation to the torsional relaxation.[38]

Fullerenes have been recently well-investigated molecules;[44−49] in particular, C_{60} has been widely used for electron-transfer systems as an electron acceptor.[50−56] We previously reported that photoexcited fullerenes (C_{60} or C_{70}) accept electrons from *n*T's when they are mixed in polar solvents;[52] it was revealed that the intermolecular ET process takes place via the triplet excited states of fullerenes and *n*T's, depending on the irradiated light. More recently, our group has already reported the intramolecular charge- and energy-transport dynamics in oligothiophene−fullerene linked dyads (*n*T-C_{60}) using pico- and nanosecond time-resolved techniques.[53,54] The charge-separation

* To whom correspondence should be addressed: E-mail: araki@tagen.tohoku.ac.jp.
† Tohoku University.
‡ Hiroshima University.
§ Present address: RIKEN, Wako, Saitama, Japan.

10.1021/jp710115z CCC: $40.75
Published on Web 01/23/2008

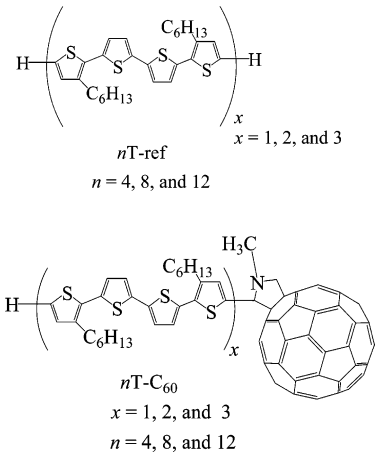

Figure 1. Molecular structures of oligothiophenes and oligothiophene-C_{60} linked dyads.

(CS) process takes place efficiently via the singlet excited states of the *n*T's and C_{60}. The charge-recombination (CR) processes take place with fast and slow components. From the slow decay, lifetimes of the radical ion pair of *n*T-C_{60} dyads were evaluated to be longer than 10^{-6} s in polar solvents. It was revealed that the slow CR process of these dyads falls in the Marcus inverted region.[58−62] The intramolecular relaxation dynamics after C_{60} excitation were investigated in detail. However, since the energy and electron-transfer processes from the lowest excited-state of the *n*T moiety (^{1}*n*T*) were quite fast and could not be detected with picosecond time resolution, the excited energy-relaxation processes from ^{1}*n*T*-C_{60} were not investigated well. Therefore, it is quite necessary to ensure the behavior of ^{1}*n*T* in the *n*T-C_{60} dyads in a femtosecond time resolution.

In this paper, we report intramolecular energy-transfer dynamics of *n*T-C_{60} (n = 4, 8, and 12 in Figure 1) by using fluorescence up-conversion method. A remarkable difference of sub-picosecond dynamics between the blue wing and the red wing of the *n*T fluorescence band was observed in longer oligothiophenes of reference compounds without the C_{60} moiety, 8T-ref and 12T-ref. Moreover, the fluorescence of the 8T and 12T moieties in the *n*T-C_{60} dyads provided the double exponential decay, while the time profile of the fluorescence of ^{1}4T*-C_{60} consists of a single decay component. On the basis of these results, we disclose the initial excitation transport dynamics in *n*T-C_{60}.

2. Experimental Section

2.1. Materials. Syntheses of the oligothiophene−fullerene linked dyads (*n*T-C_{60}), *N*-methylpyrrolidino-C_{60} (NMPC_{60}), and oligothiophenes (*n*T-ref's) were described in our previous papers.[10,11] Other chemicals (toluene and benzonitrile (PhCN)) were of the best grade commercially available.

2.2. Measurements. Steady-state absorption spectra were measured on a JASCO V-530 UV−vis spectrophotometer. Steady-state fluorescence spectra were measured on a Shimadzu RF-5300 PC spectrofluorophotometer.

As for the setup of our up-conversion fluorescence measuring systems, the light source was a mode-locked Ti:sapphire laser (Spectra-Physics, Tsunami 3950-L2S, fwhm < 150 fs) pumped with a diode-pumped solid-state laser (Spectra-Physics, Millennia VIs, 6.0 W). The oscillator produced an 82-MHz pulse train with 1.0 W average power in a fixed range of 800 nm. The fundamental pulse (λ = 800 or 820 nm) was used as a gate pulse in the up-conversion process. The second-harmonic (SH) pulse (λ = 400 or 410 nm) was generated in a 0.4 mm-thick LiB_3O_5 (LBO) crystal, which was used for a pump beam for photoexcitation. To avoid polarization effect, the angle between the polarizations of the excitation and gate beams was set to the magic angle by a $\lambda/2$ plate. The optical path of the sample cell was 1 mm, and the typical optical density of the sample at the excitation wavelength was ~0.5. The fluorescence emitted from a sample was collected and focused into a 0.4 mm thick β-BaB_2O_4 (BBO) crystal, which was mixed with the gate pulse. The gate beam and fluorescence interacted nonlinearly in a BBO crystal, and the up-converted signal was generated at the phase-matching angle. The signal was separated by a monochromator and detected by a photomultiplier tube (Hamamatsu, R-4220P) with a photon counter (Stanford Research System, SR400). The time resolution of measurements was estimated as 270 fs from the full width at half-maximum (fwhm) of the cross-correlation trace between the pump and gate pulses. The up-converted signal was accumulated for 10 s for each time-delay step. To pick up the up-converted signal from the SH scattering generated from BBO due to the gate pulse, the optical light chopper was settled in the sample excitation beam line. The light was chopped at 500 Hz, and the signal was counted at this rate.

3. Results and Discussion

3.1. Steady-State Absorption and Fluorescence Spectra. Figure 2 shows the steady-state absorption spectra of *n*T-C_{60} and their components (*n*T-ref's and NMPC_{60}) in toluene. As mentioned in our previous reports,[54] the electronic interaction between the components can be ignored in 8T-C_{60} and 12T-C_{60}, because the superposition of the component spectra is in good agreement with the spectrum of the dyad. However, the absorption band in the 400−450 nm region of the 4T moiety of 4T-C_{60} slightly shifted to the red region compared with the summed spectrum, indicating a weak electronic interaction between the components.[53] The steady-state fluorescence spectra of *n*T-ref's are also displayed in Figure 2.

Figure 3 depicts the steady-state fluorescence spectra of 12T-ref and 12T-C_{60} in toluene with 420-nm light excitation. The fluorescence band of the C_{60} moiety appeared at 720 nm, which indicates that energy transfer from 12T to C_{60} takes place as already reported.[54] In PhCN, this fluorescence due to C_{60} was not detected because the CS process takes place from 12T-$^1C_{60}$*. In 4T-C_{60} and 8T-C_{60}, similar spectral behavior due to energy transfer and electron transfer was observed.

3.2. Time Traces of Fluorescence. *3.2.1. Fluorescence Time Profiles of nT-ref.* Figure 4 depicts time traces of the fluorescence of 4T-ref in PhCN at a blue wing (460 nm) and red wing (530 nm). Figure 4a shows the fluorescence temporal profile at 460 nm, in which global-fitting analysis was demonstrated with a sum of two exponential-decay functions (eq 1).

$$I_{FL}(t) = \left[\sum_n A_n \exp(-t/\tau_n)\right] \otimes F(t) \qquad (1)$$

Hereby A_n is amplitude, and τ_n is decay time-constant. $F(t)$ was a constant term convoluted with instrumental response in the Gaussian form as experimentally estimated by the cross correlation of the gate and pump pulses with 270-fs fwhm. Although only the initial part shorter than 17 ps is shown in Figure 4a, two time-constants were found to be 4.5 and 390 ps as listed in Table 1. The slower component is assignable to the lifetime of the S_1 state to the ground state. For the fluorescence time profile at 530 nm shown in Figure 4b, the rise of the intensity can be fitted with a time constant of ca. 5 ps, which

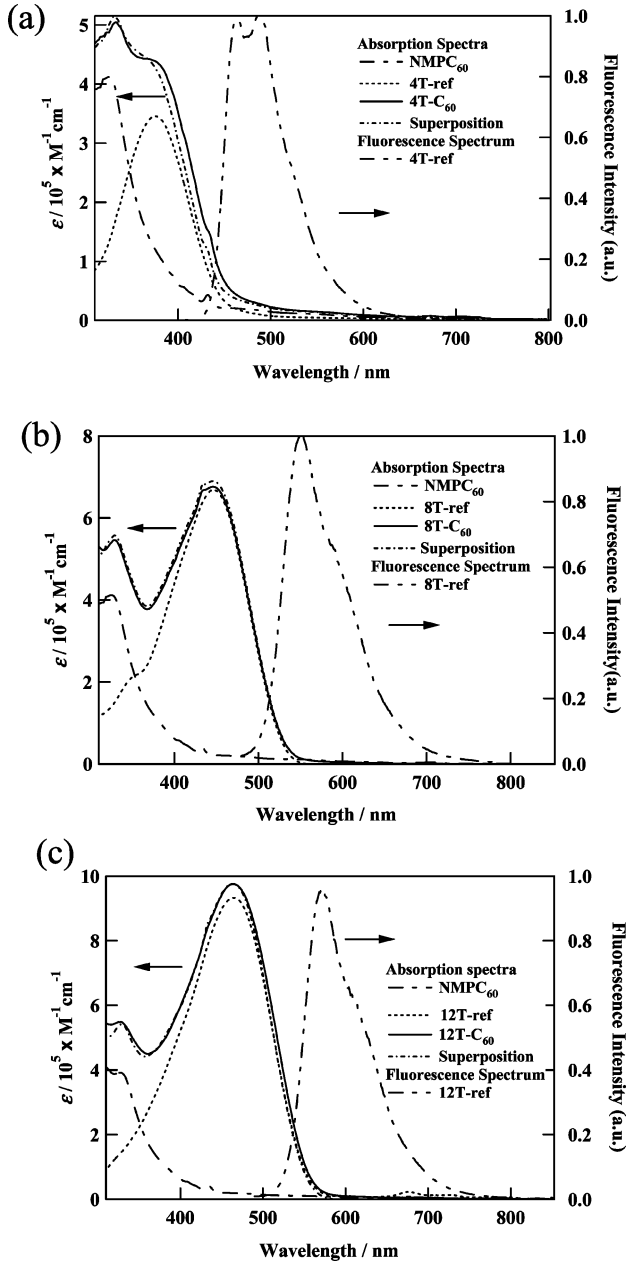

Figure 2. Steady-state absorption spectra in toluene. (a) 4T-C_{60}, (b) 8T-C_{60}, and (c) 12T-C_{60}. Their components are also displayed. Dash−dot lines indicate steady-state fluorescence spectra of *n*T-ref in toluene with 400-nm excitation.

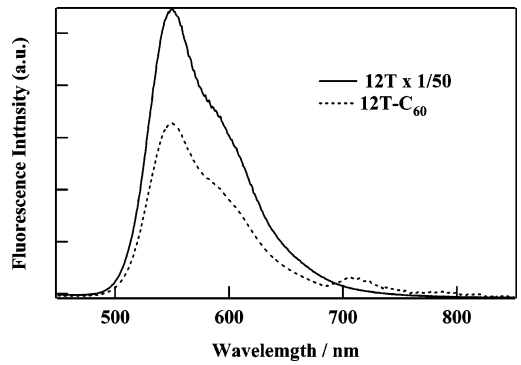

Figure 3. Steady-state fluorescence spectra corresponding to 12T-ref and 12T-C_{60} in toluene with 400-nm excitation.

is similar to the initial decay constant at 460 nm. This observation indicates that the spectral red shift takes place within

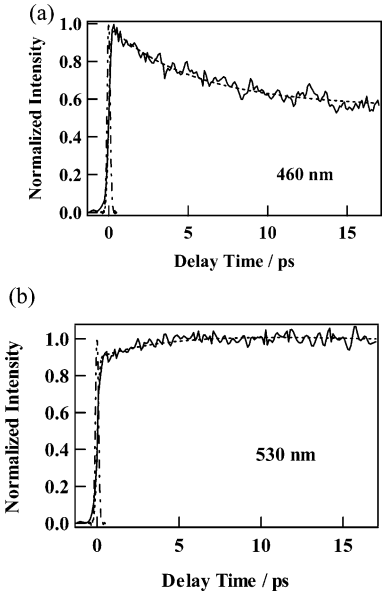

Figure 4. Time traces of the fluorescence of 4T-ref in PhCN observed with 400-nm excitation: (a) fluorescence at 460 nm and (b) fluorescence at 530 nm. Dashed and dash−dot lines are the best-fitted curve and the instrumental response, respectively.

ca. 5 ps. In toluene, the spectral red shift takes place within ca. 3 ps (Table 1). It was revealed that the shorter time constants depend on the solvent viscosity, toluene (0.587 cp), and PhCN (1.24 cp), in agreement with the similar viscosity dependence reported for fast fluorescence decay components with time constants of a few picoseconds of hexamethyl sexiththiophene.[36] Furthermore, a 4-ps component due to the torsional relaxation was also reported for the β-methyl 4T derivative.[37] Therefore, this short component obtained for the present 4T-ref can be assigned to a torsional relaxation from a flexible ground-state structure to a more rigid planar structure,[36−39] accompanying an electronic change from an aromatic character to a quinoidal character.[35] In our experiments, the femtosecond component was not observed due to our instrumental response limitation, because the self-localization of exciton coupling to the initial vibrational relaxation is expected to take place within 100 fs,[13,24,25] which was beyond the time resolution of our experimental setup.

As displayed in Figure 5, however, fluorescence dynamics of 12T-ref shows different behavior from that of 4T-ref. At a blue wing of the fluorescence band near 520 nm, the time profile with faster decay components was observed as shown in Figure 5a, which was curve-fitted with three-decay components with time constants 600 fs, 10 ps, and 620 ps in PhCN; a similar tendency was observed in toluene (Table 1). On the other hand, as shown in Figure 5b, the fluorescence time profile of the red wing at 620 nm did not provide apparently slow rise component as observed for 4T-ref at the red wing in Figure 4b. As changing the probed wavelength from the blue wing to the red wing, the initial rapid decay seems to vanish giving a single-exponential decay at 620 nm. The most proper explanation of this behavior is the cancellation of the sub-picosecond rise with picosecond-decay components at 620 nm. For the assignment of the τ_1 component of 12T-ref, we must consider two possibilities: (1) the vibrational relaxation process and (2) the EET process between segments of the 12T moiety. Since the observed τ_1 component of 12T-ref (0.6 ps) is longer than the expected vibrational relaxation time within 0.1 ps in polythiophenes,[25] possibility (1) can be ruled out. Thus, the τ_1 component with 0.6 ps is assigned to the EET between the segments of the 12T

TABLE 1: Time Constants and Their Amplitudes for the Time Trace of Fluorescence of *n*T-ref in Toluene and PhCN

solvent	sample		τ_1/ps (*A*/%)	τ_2/ps (*A*/%)	τ_3/ps (*A*/%)
toluene	4T-ref	460 nm		3.2 ± 1.0 (43%)	390 ± 30 (57%)
		530 nm		2.6 ± 1.0 (10%)[a]	390 ± 30 (90%)
	8T-ref	520 nm	0.58 ± 0.20 (53%)	3.8 ± 1.0 (34%)	610 ± 30 (13%)
		620 nm	-	5.2 ± 3.0 (17%)	610 ± 25 (83%)
	12T-ref	520 nm	0.62 ± 0.20 (53%)	4.7 ± 3.0 (33%)	600 ± 20 (14%)
		620 nm	-	8.8 ± 4.2 (14%)	600 ± 30 (86%)
PhCN	4T-ref	460 nm		4.5 ± 1.0 (40%)	390 ± 30 (60%)
		530 nm		5.5 ± 1.2 (14%) [a]	390 ± 30 (86%)
	8T-ref	520 nm	0.66 ± 0.23 (52%)	5.8 ± 1.0 (34%)	620 ± 30 (14%)
		620 nm	-	7.3 ± 2.0 (17%)	620 ± 30 (83%)
	12T-ref	520 nm	0.62 ± 0.20 (53%)	6.7 ± 3.0 (33%)	600 ± 20 (14%)
		620 nm	-	9.5 ± 4.0 (14%)	600 ± 20 (86%)

[a] Rise component.

moiety (possibility (2)), because a longer thiophene chain such as 12T-ref is expected to have the partially twisted structure, making locally π-conjugative segments in 12T. Such twisting may be induced by the *n*-hexyl chains connected at the β-position of the thiophene rings (Figure 1). This feature contributes to the inhomogeneous broadening of the absorption bands.[24] Therefore, the 400-nm light can be resonant with the blue sides of the absorption bands in 8T and 12T, indicating that higher energy segment sites of 8T and 12T are selectively excited. To verify the assignment of 0.6-ps component, the time-dependent fluorescence-anisotropy measurement ($r(t)$) of 12T-ref was performed as shown in Figure 6, in which the anisotropy decay $r(t)$ is given by eq 2.

$$r(t) = \frac{I_{\parallel}(t) - GI_{\perp}(t)}{I_{\parallel}(t) + 2GI_{\perp}(t)} \qquad (2)$$

Hereby, $I_{\parallel}(t)$ and $I_{\perp}(t)$ are the fluorescence decay curves recorded with the parallel and perpendicular polarization of the excitation pulse. G is a polarization bias (1.32). In Figure 6, a rapid anisotropy decay component was observed, giving the time constant to be 560 fs. Similar anisotropy decay was already reported in polythiophene, corresponding to the EET among the thiophene segments.[14] Therefore, the τ_1 component can be assignable to the EET process between the locally π-conjugative segments of the 12T moiety. Furthermore, the energy level of the S_1 state of the segments goes down with increasing the length of the π-conjugation.[27−29] As a consequence, the EET takes place from higher energy short segments to lower energy long segments. 8T-ref is also expected to have the locally π-conjugative segments, as the blue wings of the steady-state absorption and fluorescence of 8T-ref overlapped with the main peaks of 4T-ref. In the case of 4T, however, the π-conjugation spreads over almost four thiophene rings acting as a chromophore; thus, the ultrafast component was not observed.

In 12T-ref, the other two components, τ_2 and τ_3, can be assigned to the torsional relaxation dynamics and the internal conversion from the S_1 state, respectively. Apparently, the solvent-viscosity dependence of the τ_2 component affords a support for the assignment to the torsional relaxation similar to the shorter component of 4T-ref. In 8T-ref, three time constants were also evaluated as listed in Table 1. These three time constants can be assigned to the EET process between segments, the torsional relaxation dynamics, and the lifetime of the S_1 state of 8T-ref on the analogy of 12-ref.

The small wavelength dependence of the τ_2 values was also observed as listed in Table 1, which may be caused by the dynamic red shift of the fluorescence band accompanied with the structural relaxation process in agreement with the hypothesis presented by Sundström and co-workers.[14−16,38] Moreover, the τ_2 values slightly depend on the total *n*T's length in addition to the probe wavelength (Table 1), suggesting that the torsional motion of the longer chain in this conformational relaxation is more strongly restricted by the friction with solvent molecules.

TABLE 2: Time Constants for the Time Trace of Fluorescence of 4T-C_{60} in Toluene and PhCN

solvent		τ_1/ps (*A* %)
toluene	460 nm	0.28 ± 0.10 (100%)
	530 nm	0.31 ± 0.12 (100%)
PhCN	460 nm	0.33 ± 0.10 (100%)
	530 nm	0.26 ± 0.09 (100%)

SCHEME 1

$$4T\text{-}C_{60} \xrightarrow{h\nu} {}^1 4T^*\text{-}C_{60} \xrightarrow[\sim 300\ fs]{EET} 4T\text{-}{}^1C_{60}^*$$

3.2.2. Fluorescence Time Profiles of nT-C_{60}. 4T-C_{60}. Figure 7a shows the time traces for the fluorescence of the 4T moiety in 4T-C_{60} in toluene. The decay of the fluorescence intensity was much faster than that of 4T-ref, indicating that the EET takes place from ^{1}4T* to C_{60}. Time constants evaluated by single-exponential fitting are in the 260−330-fs region as summarized in Table 2, in which the slight wavelength dependence and the solvent dependence of the decay time constants are within the experimental error. These time constants can be attributed to the EET from ^{1}4T* to C_{60}, which occurs before the torsional relaxation of ^{1}4T*-ref within 3−5 ps (Table 1) as represented by Scheme 1.

To check the validity of this assignment, the up-converted signal of the fluorescence at 700 nm due to C_{60} in 4T-C_{60} was monitored (Figure 7b). The signal grew up with a 300-fs time constant was observed in agreement with the decay time constant of 4T, supporting that the EET from the 4T moiety to the C_{60} moiety takes place predominately.

12T-C_{60} and 8T-C_{60}. Time traces of the fluorescence of 12T-C_{60} at 520 and 620 nm in toluene are displayed in Figure 8a. The fluorescence transients of 12T-C_{60} at blue and red wings decayed faster than those of 12T-ref. The fluorescence dynamics of both wings consists of two stages; a sub-picosecond component (ca. 0.5 ps) and a picosecond component (ca. 5 ps); see Supporting Information, Table S1. As shown in Figure 8b, the rise profile of the fluorescence at 700 nm mainly due to the C_{60} moiety also consists of two stages. Thus, these observations indicate that the EET takes place from the 12T moiety to the C_{60} moiety. As seen in Figure 8a, the persisting tail of fluorescence at 620 nm decays slower than that at 520 nm. This difference indicates that the longer segment mainly contributing to the red wing of the fluorescence band shows slower EET compared with the shorter segment at blue wing in the picosecond components.

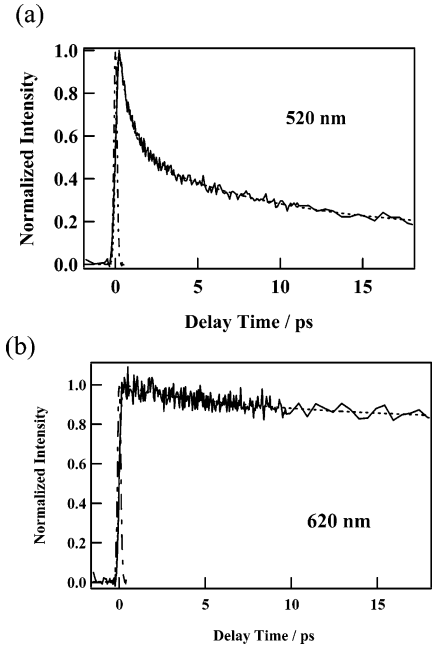

Figure 5. Time traces of the fluorescence of 12T-ref in PhCN observed with 400-nm excitation: (a) fluorescence at 520 nm and (b) fluorescence at 620 nm. Dashed and dash−dot line are the best-fitted curve and the instrumental response, respectively.

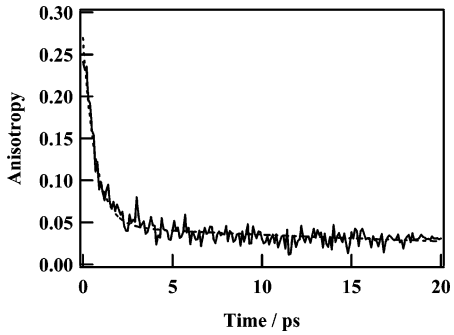

Figure 6. Fluorescence anisotropy time trace of 12T-ref at 520 nm in PhCN observed with 400-nm excitation; anisotropy is defined as eq 2 in text. Dashed line is the best-fitted curve.

On the basis of these observations, three models can be proposed for the explanation of the EET dynamics in 12T-C_{60} as shown in Figure 9. The presence of three types of EET from the lower energy segment to C_{60} can be rationalized by considering three types of relative positions of the segments with respect to C_{60}. The short time constant may be for near-side positions and the longer time constant for far-side positions as will be discussed in the next section. Since the picosecond components (ca. 5 ps) were observed for 12T-C_{60} but not for 4T-C_{60}, these longer components may correspond to the segment positioned far from the C_{60} moiety at least by the 4T unit.

The time traces of the fluorescence of ^{1}8T*-C_{60} also decay with biexponential kinetics (see Supporting Information, Figure S1). From the biexponential curve fitting, sub-picosecond time constants (ca. 0.4 ps) and picosecond time constants (ca. 3−4 ps) were evaluated (see Supporting Information, Table S1), which can be attributed to EET from the segments of the ^{1}8T* moiety to the C_{60} moiety. These observed fluorescence time profiles can be analyzed on the basis of the kinetic models similar to 12T-C_{60} as illustrated in Figure 9, although the lengths of the segments of 8T-C_{60} may be shorter than those of 12T-C_{60}.

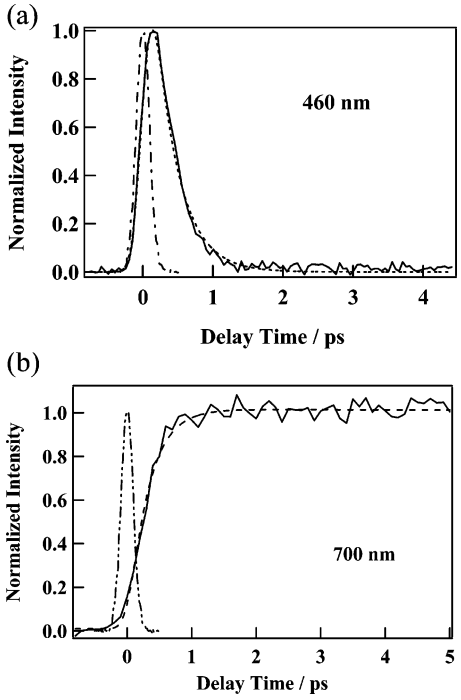

Figure 7. Fluorescence decay of 4T-C_{60} in toluene (a) at 460 nm with 400-nm excitation and (b) at 700 nm with 410-nm excitation. Dashed and dash−dot lines are the best-fitted curve and the instrumental response, respectively.

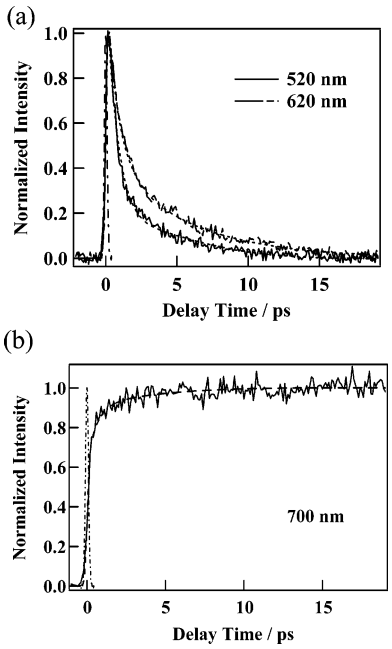

Figure 8. Fluorescence decays of 12T-C_{60} in toluene observed (a) at 520 and 620 nm with 400-nm excitation and (b) at 700 nm with 410-nm excitation. Dashed and dash-dot lines are the best-fitted curve and the instrumental response, respectively.

3.3. Kinetic Analysis of EET Rates in 12T-C_{60} and 8T-C_{60}. As shown in Figure 9 for 12T-C_{60}, a longer π-conjugated segment (LT) is located near the C_{60} moiety in type A, whereas a shorter π-conjugated segment (ST) is located near the C_{60} moiety in type B; furthermore, a relatively long π-conjugative unit is located in the center position of 12T in type C. Figure 10 depicts the schematic energy diagrams accompanying the photoinduced energy-transfer processes for 12T-C_{60}. Our kinetic simulations need the following three postulations: (1) the EET process within oligothiophenes takes place via the Förster

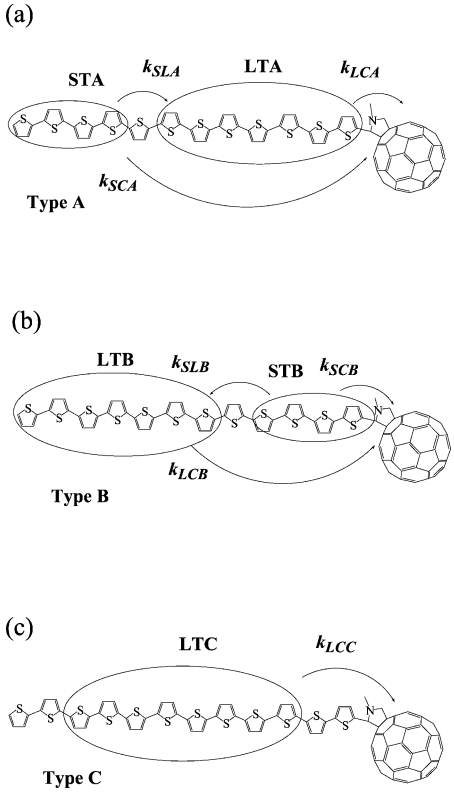

Figure 9. EET models of 12T-C_{60}, including the relevant EET rate parameters (also see parts a and b of Figure 10). Arrows indicate EET pathways. ST refers to shorter thiophene segment and LT refers to longer thiophene segment. Suffix C is an abbreviation of C_{60}.

incoherent energy hopping mechanism,[63] similar to polythiophenes,[14−26] (2) the time constants (rate constants) are ensemble averages of the segments with trifling distributions, and (3) the population of the S_1 state of 12T goes back to the ground state with EET to C_{60} within 15 ps as seen in Figure 8a, that is, no participation of torsional relaxation dynamics of the S_1 state with the lifetime of 600 ps for 12T-ref. Then, time-dependent total population ($P_{total}(t)$) of the ^{1}12T* moiety in 12T-C_{60} moiety is given by eq 3.

$$P_{total}(t) = P_{ST}(t) + P_{LT}(t) = a_1\{P_{STA}(t) + P_{LTA}(t)\} + a_2\{P_{STB}(t) + P_{LTB}(t)\} + a_3P_{LCC}(t) \quad (3)$$

Here, $P_{ST}(t)$ and $P_{LT}(t)$ mean the probabilities of ST and LT in the S_1 states, respectively, which are sum of $P_{STA}(t)$ and $P_{LTA}(t)$ for type A, sum of $P_{STB}(t)$ and $P_{LTB}(t)$ for type B, and $P_{LCC}(t)$ for type C in Figure 10. In eq 3, coefficients a_i indicate initial population fractions. By employment the rate parameters as defined in Figures 9 and 10, the fitting function ($I(t)$) for the ^{1}12T* part is given by eq 4.

$$I(t) = A_1\exp(-(k_{SCA} + k_{SLA})t) + A_2\exp(-(k_{SCB} + k_{SLB})t) + A_3\exp(-k_{LCC}t) - A_4\{\exp(-(k_{SCA} + k_{SLA})t)\} - A_5\{\exp(-(k_{SCB} + k_{SLB})t)\} + A_6\exp(-k_{LCA}t) + A_7\exp(-k_{LCB}t) \quad (4)$$

Here, coefficients A_i refer as to the amplitudes for the kinetic components, and the positive sign indicates the decay feature, while the minus sign means the rise kinetics (for details, see Supporting Information, eq S11). By use of eq 4, the curve-fitting analysis was carried out. The best-fitted curves are displayed in Figure 8. Since the electronic interaction between the 12T and C_{60} moieties is negligibly small due to the similarities of the absorption and fluorescence bands to those of 12T-ref, it is reasonable to employ the $1/\tau_1$ (1.7×10^{12} s^{-1}) value of 12T-ref as for k_{SLA} and k_{SLB}. The instrumental response was also considered in this simulation by adopting a Gaussian function having a time resolution of 270 fs. The obtained time constants are listed in Table 3, in which the solvent effect is very small. It is also notable that these time constants are independent from the monitoring wavelength; that is, the observed slight difference of the fluorescence decay tail with monitoring wavelength must come from other factors such as A_i. In type A, τ_{LCA} (ca. 1 ps) is shorter than τ_{SCA} (ca. 5 ps), suggesting that EET from short distance segment is higher priority to that from the distant higher energy segment. The shortest time constant is τ_{SCB} (0.42−0.43 ps), which is quite reasonable on taking both high energy and the short distance into consideration (type B). In addition, the order of $\tau_{LCB} > \tau_{LCC}$ is also reasonable due to longer distance of LCB compared with LCC in Figure 9.

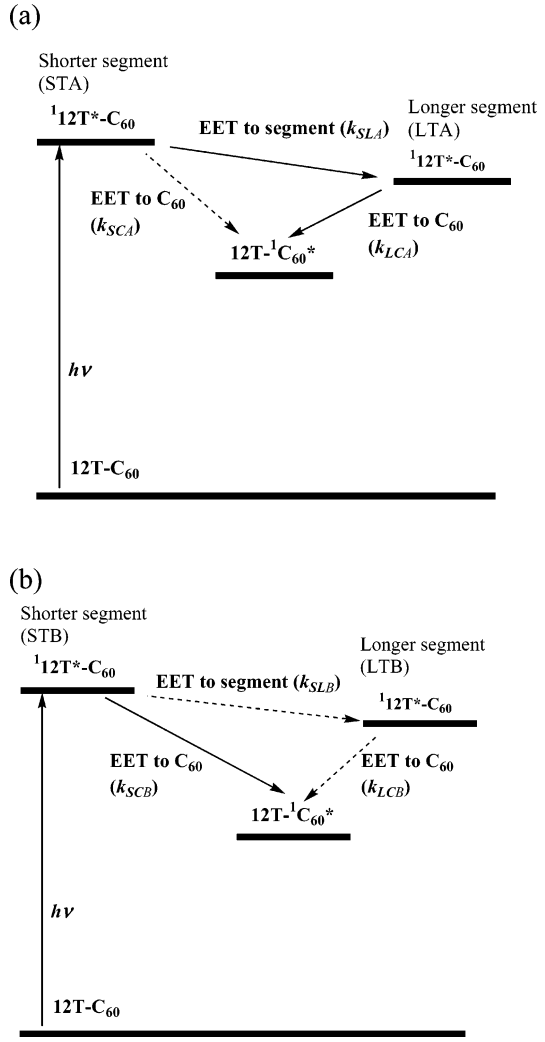

Figure 10. Schematic energy diagrams for 12T-C_{60}; (a) and (b) indicate reaction paths for model A and model B of Figure 9, respectively.

The sums of amplitudes A_1-A_3 are almost 100% as listed in Table 4; a fraction of type A is major (about 60%), whereas the fraction of type B is minor (20−36%), and the contribution of type C is negligibly small. Other amplitudes A_4-A_7 are listed in Supporting Information (Table S2). In combination with the shorter time process (τ_{LCA}) in type A, the main process for 12T-

TABLE 3: Time Constants for EET in 8T-C_{60} and 12T-C_{60} in Toluene and PhCN[a]

solvent	sample	τ_{SCA}/ps[b]	τ_{SCB}/ps[b]	τ_{LCA}/ps[b]	τ_{LCB}/ps[b]	τ_{LCC}/ps[b]
toluene	8T-C_{60}	1.9 ± 0.23	0.39 ± 0.13	0.74 ± 0.19		1.2 ± 0.5
	12T-C_{60}	5.1 ± 0.8	0.42 ± 0.08	1.0 ± 0.14	7.0 ± 1.3	2.9 ± 1.3
PhCN	8T-C_{60}	2.1 ± 0.11	0.35 ± 0.15	0.81 ± 0.21		1.5 ± 0.7
	12T-C_{60}	5.4 ± 1.0	0.43 ± 0.10	0.90 ± 0.20	7.2 ± 1.6	3.0 ± 1.0

[a] Rate constants for EET evaluated from eqs 4 and 5; k_{SLA} and k_{SLB} were entered from the experimental results of $1/\tau_1$ of *n*T-ref. [b] Lifetimes ($\tau = 1/k$).

TABLE 4: Amplitudes (A_1−A_3) for Exponential Components in Eq 4 in 8T-C_{60} and 12T-C_{60} in Toluene and PhCN (for A_4−A_7, See Supporting Information, Table S2)[a]

solvent	sample		A_1	A_2	A_3
toluene	8T-C_{60}	520 nm	18%	73%	9%
		620 nm	17%	75%	10%
	12T-C_{60}	520 nm	65%	37%	4%
		620 nm	58%	19%	1%
PhCN	8T-C_{60}	520 nm	17%	73%	9%
		620 nm	18%	71%	10%
	12T-C_{60}	520 nm	64%	36%	4%
		620 nm	57%	18%	1%

[a] Amplitudes were determined by global fitting analysis.

C_{60} is the EET from LTA to C_{60}. It is notable that only the A_2 value is dependent on the monitoring wavelength; that is, the A_2 values evaluated from the blue wing (36−27%) are about twice those from the red wing (18−19%). Since the tail of the fluorescence transient of ^{1}12T*-C_{60} (Figure 8a) is dependent on the monitoring wavelength, the fraction of the LCB process is the main origin. The negative amplitudes were found for A_4 (20−30%), whereas positive amplitudes were found for A_6 (25−40%); A_5 and A_7 are minor. The negative A_4 term indicates the initial formation of ^{1}LTA* from ^{1}STA* ($k_{SLA} = 1/(0.62$ ps)) followed by the decay to C_{60} with EET ($k_{LCA} = 1/\tau_{LCA}$ (1 (ps)$^{-1}$). The positive A_6 term corresponds to the predominant decay of ^{1}LTB* to C_{60} via EET.

From Figure 8b, time constants were also evaluated from the fitting analysis of the rise fluorescence transient at 700 nm mainly due to C_{60} on the basis of the three types in Figure 9. The evaluated rise time constants were 0.4, 1.1, 2.6, 6.0, and 6.9 ps, which are counterparts to the decay time constants of the 12T moiety, τ_{SCB}, τ_{LCA}, τ_{LCC}, τ_{SCA}, and τ_{LCB}, respectively. However, the amplitude for the rise component with 2.6 ps was less than 2%, suggesting that EET in type C is a minor process, which is also consistent with the result from Figure 8a.

The same procedures could be also applied to 8T-C_{60}; the evaluated time constants and fractions are added to Tables 3 and 4, respectively. A fraction of type B ($A_2 = 70\%$) is predominant, and the contribution of τ_{LCB} value is too small to evaluate. The fastest process is the EET from STB to C_{60} ($\tau_{SCB} = 0.35-0.39$ ps), which is almost the same as that for 12T-C_{60}.

The order of the main fastest process with time constants τ_{SCB} for *n*T-C_{60} including τ_1 for 4T-C_{60} is given as follows: 12T-C_{60} (0.42−0.43 ps) > 8T-C_{60} (0.35−0.39 ps) > 4T-C_{60} (0.26−0.33 ps). This order for the τ_{SCB} values can be explained on the basis of the donor−acceptor distance, because the size of the STB increases as the length of *n*T increases, leading an increase in the center-to-center distance (R_{CC}) between STB and C_{60}. Since the τ_{SCB} values for *n*T-C_{60} are shorter than the τ_1 value (τ_{SLB}) at 520 nm for *n*T-ref (0.58−0.66 ps), the EET from the short segment to C_{60} mainly (k_{SCB}) occurs faster than the EET from the short segment to long segment (k_{SLB}). In the case of 12T-C_{60}, the τ_{LCC} ($1/k_{LCC}$) was found to be longer than τ_{LCB} ($1/k_{LCB}$), suggesting the presence of the long segment near the central position of *n*T. The order of $A_1 > A_2$ for 12T-C_{60} (implying type A) is opposite to that for 8T-C_{60} (predominant SCB process in type B), suggesting that 8T-C_{60} is rather similar to single decaying 4T-C_{60}.

In our previous reports,[56,57] the CS process after the energy transfer from ^{1}*n*T* to C_{60} was already discussed, in which the CS process via $^1C_{60}$* generating *n*T$^{\bullet+}$-$C_{60}^{\bullet-}$ takes place in the time range of 50 ps for 4T-$^1C_{60}$*, 100 ps for 8T-$^1C_{60}$*, and 150 ps for 12T-$^1C_{60}$*. As for CS via ^{1}*n*T*, we could deny this direct CR process in the present study, because of independence of the observed time constants for the fluorescence decay on the solvent polarity. This conclusion is supported by Lanzani and Janssen groups, since they reported that the energy transfer from ^{1}*n*T* to C_{60} of the C_{60}-*n*T-C_{60} triad predominantly occurs as fast as 97 fs.[65] They also proved that the CS state was formed via $^1C_{60}$* with a 10-ps time constant after this energy transfer.

4. Conclusion

Investigations of primary energy transfer dynamics in *n*T-C_{60} ($n = 4$, 8, and 12) via ^{1}*n*T*, which had been impossible with a conventional picosecond fluorescence technique, were achieved by using a femtosecond fluorescence up-conversion technique in the present study. Additionally, fluorescence dynamics of the oligothiophenes (4T-ref, 8T-ref, and 12T-ref) were also investigated as references, which revealed that the EET takes place from a segment to another segment in the ^{1}*n*T* moiety on a sub-picosecond time scale in longer oligothiophenes (8T-ref and 12T-ref), after which the torsional relaxation occurs on a picosecond time scale. In 4T-C_{60}, fluorescence decay of the ^{1}*n*T* moiety with single sub-picosecond time constant was observed, which is assigned to the EET from the 4T moiety to the C_{60} moiety. In 8T-C_{60} and 12T-C_{60}, sub-picosecond and picosecond decays were found in the fluorescence of the ^{1}*n*T* moiety, from which the time constants of the elemental processes were estimated on the basis of three models with different positions of the segments in 8T and 12T. These elemental time constants with the sub-picosecond time region are assignable to the EET to the C_{60} moiety from the segments near the C_{60} moiety, with which EET along the segments of the ^{1}*n*T* moiety takes place simultaneously. In addition, picosecond energy transfer was found in 8T-C_{60} and 12T-C_{60}, which was attributed to the EET from the segments in the ^{1}*n*T* moiety apart from the C_{60} moiety.

Acknowledgment. This work was supported by the 21st Century Center of Excellence program "Giant Molecule and Complex Systems" for Tohoku University.

Supporting Information Available: Derivatives of kinetic equations. This material is available free of charge via the Internet at http://pubs.acs.org.

References and Notes

(1) Mitschke, U.; Bäuerle, P. *J. Mater. Chem.* **2000**, *10*, 1471.
(2) Shirota, Y. *J. Mater. Chem.* **2000**, *10*, 1.

(3) Harrison, M. G.; Friend R. H. In *Electronic Materials: The Oligomer Approach*; Müllen, K., Wegner, G., Eds.; Wiley-VCH: Weinheim, 1998; pp 515−558.
(4) van Duren, J. K. J.; Dhanabalan, A.; van Hal, P. A.; Janssen, R. A. J. *Synth. Met.* **2001**, *121*, 1587.
(5) Horowitz, G.; Adv. Mater. **1998**, *10*, 365.
(6) Dimitrakopoulos, C. D.; Malenfant, P. R. M. *Adv. Mater*. **2002**, *14*, 99.
(7) Nalwa, H. S. In *Handbook of Organic Conductive Molecules and Polymers*; Nalwa, H. S., Ed.; John Wiley: Chichester, 1997; Vol. 4, pp 261−363.
(8) Nakanishi, H.; Aso, Y.; Otsubo, T. *Synth. Met.* **1999**, *101*, 413.
(9) Nakanishi, H.; Sumi, N.; Ueno, S.; Takimiya, K.; Aso, Y.; Otsubo, T.; Komaguchi, K.; Shiotani, M.; Ohta, N. *Synth. Met.* **2001**, *119*, 413.
(10) Otsubo, T.; Aso, Y.; Takimiya, K. *Bull. Chem. Soc. Jpn.* **2001**, *74*, 1789.
(11) Otsubo, T.; Aso, Y.; Takimiya, K. *J. Mater. Chem.* **2002**, *12*, 2565.
(12) Yalikaraki, S. N.; Silbey, R. J. *J. Chem. Phys.* **1996**, *104*, 1245.
(13) Heun, S.; Mahrt, R. F.; Greiner, A.; Lemmer U.; Bässler, H.; Halliday, D. A.; Bradley, D. D. C.; Burn, P. L.; Holmes, A. B. *J. Phys. Condens. Matter* **1993**, *5*, 247.
(14) Beenken, W. J. D.; Pullerits, T. *J. Chem. Phys.* **2004**, *120*, 2490.
(15) Westenhoff, S.; Daniel, C.; Friend, R. H.; Silva, C.; Sundström, V.; Yartsev, A. *J. Chem. Phys.* **2005**, *122*, 094903.
(16) Westenhoff, S.; Beenken, W. J. D.; Friend, R. H.; Greenham, N. C.; Yartsev, A.; Sundström, V. *Phys. Rev. Lett.* **2006**, *97*, 166804.
(17) Kersting, R.; Lemmer, U.; Mahrt, R. F.; Leo, K.; Kurz, H.; Bässler, H., Göbel, E. O. *Phys. Rev. Lett.* **1993**, *70*, 3820.
(18) Kersting, R.; Mollay, B.; Rusch, M.; Wenisch, J.; Leising, G.; Kauffman, H. F. *J. Chem. Phys.* **1996**, *106*, 2850.
(19) Bock, A. M.; Schmid, D.: Kryschi, C. *J. Chem. Phys.* **1999**, *111*, 1185.
(20) Tretiak, S.; Saxena, A.; Martin, R. L.; Bishop, A. R. *Phys. Rev. Lett.* **2002**, *89*, 097402.
(21) Beljonne, D.; Pourtois, G.; Silva, C.; Hennebicq, E.; Herz, L. M.; Friend, R. H.; Scholes, G. D.; Setayesh, S.; Müllen, K.; Brédas, J. L. *PNAS* **2002**, *99*, 10983.
(22) Grage, M. M.-L.; Zaushitsyn, Y.; Yartsev, A.; Chachisvilis, M.; Sundström, V.; Pullerits, T. *Phys. Rev. B* **2003**, *67*, 205207.
(23) Grage, M. M.-L.; Wood, P. W.; Ruseckas, A.; Pullerits, T.; Mitchell, W.; Burn, P. L.; Samuel, I D. W.; Sundström, V. *J. Chem. Phys.* **2003**, *118*, 7644.
(24) Beenken, W. J. D.; Pullerits, T. *J. Phys. Chem. B* **2004**, *108*, 6164.
(25) Dykstra, T. E.; Kovalevskij, V.; Yang, X.; Scholes, G. D. *Chem. Phys.* **2005**, *318*, 21.
(26) Beljonne, D.; Hennebicq, E.; Daniel, C.; Herz, L. M.; Silva, C.; Scholes, G. D.; Moeben, F. J. M.; Jonkheijm, P.; Schenning, A. P. H.; Meskers, S. C. J.; Phillips, R. T.; Friend, R. H.; Meijer, E. W. *J. Phys. Chem. B* **2005**, *109*, 10594.
(27) Becker, R. S.; de Melo, J. S.; Maçantia, A. L.; Elisei, F. *Pure Appl. Chem.* **1995**, *67*, 9.
(28) Becker, R. S.; de Melo, J. S.; Maçantia, A. L.; Elisei, F. *J. Phys. Chem.* **1996**, *100*, 1863.
(29) de Melo, J. S.; Silva, L. M.; Arnaut, L. G.; Becker, R. S. *J. Chem. Phys.* **1999**, *12*, 5427.
(30) Colditz, R.; Grebner, D.; Helbig, M.; Rentsch, S. *Chem. Phys.* **1995**, *201*, 309.
(31) Beljonne, D.; Cornil, J.; Friend, R. H.; Janssen, R. A. J.; Brédas, J. -L. *J. Am. Chem. Soc.* **1996**, *118*, 6453.
(32) Beljonne, D.; Shuai, Z.; Pourtois, G.; Brédas, J. -L. *J. Phys. Chem. A* **2001**, *105*, 3899.
(33) Brédas, J. -L.; Geskin, V. M. *Chem. Phys. Chem.* **2003**, *4*, 498.
(34) Fabiano, E.; Della, Sala, F.; Cingolani, R. *Phys. Status Solidi* **2004**, *3*, 539.
(35) Janssen, R. A. J.; Smilowitz, L.; Sariciftci, N. S.; Moses, D. *J. Chem. Phys.* **1994**, *101*, 1787.
(36) Lanzani, G.; Nisoli, M.; Magni, V.; De Silvestri, S.; Barbarella, G.; Zambianchi, M.; Tubino, R. *Phys. Rev. B* **1995**, *51*, 13770.
(37) Lanzani, G.; Nisoli, M.; De Silvestri, S.; Tubino, R. *Chem. Phys. Lett.* **1996**, *251*, 339.
(38) Wong, K. S.; Wang, H.; Lanzani, G. *Chem. Phys. Lett.***1998**, *288*, 59.
(39) Lanzani, G.; Cerullo, G.; Stagira, S.; De Silvestri, S. *J. Photochem. Photobiol. A* **2001**, *144*, 13.
(40) Paa, W.; Yang, J.-P.; Helbig, M.; Hein, J.; Rentsch, S. *Chem. Phys. Lett.* **1998**, *292*, 607.
(41) Paa, W.; Yang, J.-P.; Rentsch, S. *Appl. Phys. B* **2000**, *71*, 443.
(42) Yang, A.; Hughes, S.; Kuroda, M.; Shiraishi, Y.; Kobayashi, T. *Chem. Phys. Lett.* **1997**, *280*, 475.
(43) Yang, A.; Kuroda, M.; Shiraishi, Y.; Kobayashi, T. *J. Phys. Chem. B* **1998**, *102*, 3706.
(44) Kroto, H. W.; Heath, J. R.; O'Brien, S. C.; Curl, R. F.; Smalley, R. E. *Nature* **1985**, *318*, 162.
(45) Haddon, R. C. *Acc. Chem. Res.* **1988**, *21*, 243.
(46) Haddon, R. C. *Science* **1993**, *261*, 1545.
(47) Sassara, A.; Zerza, G.; Chergui, M. *J. Phys. B* **1996**, *29*, 4997.
(48) Negri, F.; Orlandi, G.; Zerebetto, F. *J Phys. Chem.* **1996**, *100*, 10849.
(49) Dauw, X. L. R.; Bronsveld, M. V.; Krüger, A.; Warntjes, J. B. M.; Witjes, M. R. *J. Chem. Phys.* **1998**, *109*, 21.
(50) Imahori, H.; Hagiwara, K.; Akiyama, T.; Aoki, M.; Taniguchi, S.; Okada, T.; Shirakawa, M.; Sakata, Y. *Chem. Phys. Lett.* **1996**, *263*, 545.
(51) Guldi, D. M.; Garscia, G. T.; Mattay, J. *J. Phys. Chem. A* **1998**, *102*, 9679.
(52) Matsumoto, K.; Fujitsuka, M.; Sato, T.; Onodera, S.; Ito, O. *J. Phys. Chem. B* **2000**, *104*, 11632.
(53) Fujitsuka, M.; Ito, O.; Yamashiro, T.; Aso, Y.; Otsubo, T. *J. Phys. Chem. A* **2000**, *104*, 4876.
(54) Fujitsuka, M.; Matsumoto, K.; Ito, O.; Yamashiro, T.; Aso, Y.; Otsubo, T. *Res. Chem. Intermed*. **2001**, *27*, 73.
(55) Tkachenko, N. V.; Rantala, L.; Tauber, A. Y.; Helaja, J.; Hynninen, P. V.; Lemmetyinen, H. *J. Am. Chem. Soc.* **1999**, *121*, 9378.
(56) Guldi, D. M.; Maggini, M.; Scorrano, G.; Prato, M. *J. Am. Chem. Soc.* **1997**, *119*, 974.
(57) Imahori, H.; Cardoso, S.; Tatman, D.; Lin, S.; Noss, L.; Seely, G. R.; Sereno, L.; Silber, C.; Moore, T. A.; Moore, A. L.; Gust, D. *J. Photochem. Photobiol. A* **1995**, *62*, 1009.
(58) Marcus, R. A. *J. Chem. Phys.* **1956**, *24*, 966.
(59) Marcus, R. A. *J. Chem. Phys.* **1957**, *26*, 867.
(60) Marcus, R. A. *J. Chem. Phys.* **1957**, *26*, 872.
(61) Marcus, R. A. *J. Chem. Phys.* **1965**, *43*, 679.
(62) Marcus, R. A.; Sutin, N. *Biochim. Biophys. Acta* **1985**, *811*, 265.
(63) Förster, T. *Ann. Chem.* **1948**, *2*, 55.
(64) Scheblykin, I. G.; Yartsev, A.; Pullerits, T.; Gulbinas, V.; Sundström, V. *J. Phys. Chem. B* **2007**, *111*, 6303.
(65) van Hal, P. A.; Janssen, R. A. J.; Lanzani, G.; Cerullo, G.; Zavelani-Rossi, M.; De Silvestri, S. *Chem. Phys, Lett.* **2001**, *345*, 33.